34th Annual International Conference of the IEEE EMBS
San Diego, California USA, 28 August - 1 September, 2012

Decoding Hand Trajectories from Micro-Electrocorticography in Human Patients

Spencer Kellis, Sara Hanrahan, Tyler Davis, Paul A. House, Richard Brown, and Bradley Greger

***Abstract*—A Kalman filter was used to decode hand trajectories from micro-electrocorticography recorded over motor cortex in human patients. In two cases, signals were recorded during stereotyped tasks, and the trajectories were decoded offline, with maximum correlation coefficients between actual and predicted trajectories of 0.51 (x-direction position) and 0.54 (y-direction position). In a third setting, a human patient with full neural control of a computer cursor acquired onscreen targets within 6.24 sec on average, with no algorithmic constraints on the output trajectory. These practical results illustrate the potential utility of signals recorded at the cortical surface with high spatial resolution, demonstrating that surface potentials contain relevant and sufficient information to drive sophisticated brain-computer interface systems.**

I. Introduction

Micro-electrocorticography (μEcoG) provides more spatial resolution than what is currently possible with electroencephalography (EEG) or standard electrocorticography (EcoG) grids [1]. Because the electrodes are smaller, they have different physical properties, such as higher electrical impedances, than standard ECoG recording electrodes. These electrical properties require different amplification and signal analysis capabilities than those available with clinical EEG recording equipment [2]. μECoG can serve as a platform to chronically record local field potential signals from the surface of the neocortex which contain sufficient information to decode a relatively stereotyped movement [3]. One benefit of μEcoG grids is that they can be safely placed over eloquent cortex and used to decode complex movements such as speech [4]. These qualities of μEcoG grids make them well suited for implementing online decodes of continuous movements, which allows the patient to make use of visual feedback of performance during the task [5].

Here we present performance and analysis of the decoding of hand trajectories from local field potentials recorded using μEcoG grids. In two patients the decoding was performed offline. These data exhibited above-chance performance despite the lack of visual feedback for online error correction. In a third patient, decoding was performed online with closed-loop visual observation of performance. These data demonstrate the potential for real-time control via a μEcoG cortical interface. All three datasets show that μECoG grids can serve as a platform for neural prosthetic applications.

This work was supported in part by the Engineering Research Center Program of the National Science Foundation under award number EEC-9986866), and by DARPA BAA05-26 Revolutionizing Prosthetics.

S. Kellis is with the Division of Biology, California Institute of Biology, Pasadena, CA 91125 USA (e-mail: spencer.kellis@caltech.edu).

S. Hanrahan, T. Davis, and B. Greger are with the Dept. of Bioengineering, University of Utah, Salt Lake City, UT 84112 USA (emails: s.hanrahan@utah.edu, tyler.davis@hsc.utah.edu, bradley.greger@utah.edu).

P. A. House is with the Department of Neurosurgery, University of Utah, Salt Lake City, UT 84132 USA (e-mail: paul.house@hsc.utah.edu).

R. Brown is with the Department of Electrical and Computer Engineering, the School of Computing, and the Department of Bioengineering, University of Utah, Salt Lake City, UT 84112, USA (e-mail: brown@utah.edu).

II. Methods

A. Subjects

Three male patients requiring long-term electrocorticographic monitoring for medically refractory epilepsy were enrolled in an Institutional Review Board-approved protocol. Informed consent was obtained from each patient.

Patient one (P1) was implanted with two 16-channel μECoG grids (40-micron wire) (PMT Corporation, Chanhassen, MN) with 1-mm interelectrode spacing, placed in the epipial space underneath a standard clinical ECoG grid (Fig. 1). One of the arrays was placed over upper extremity primary motor cortex as confirmed with intraoperative somatosensory evoked potential (SSEP) monitoring. The other array was placed more inferiorly along the precentral gyrus. Both arrays were referenced to a pair of epidural bare wires. Patient two (P2) was implanted with a single 30-channel μECoG grid with 2-mm interelectrode spacing. The anterior portion of the array was placed over the hand area of primary motor cortex as confirmed using extraoperative electrical stimulation with electromyographic confirmation. The array was referenced to two low-impedance electrodes built into the device. Patient three (P3) was implanted with a single 64-channel μECoG grid (50-micron wire) (Ad-Tech Medical Instrument Corporation, Racine, WI) with 3-mm interelectrode spacing, placed over hand and arm sensory and motor cortex. The array was referenced to an EEG scalp electrode.

B. Experimental Paradigm

Patients P1 and P2 were instructed to perform simple, repetitive movements to move a computer mouse with arm and hand contralateral to the implanted electrodes. On verbal cue, the patient moved the mouse from a starting position, at the bottom center of the tablet, to the upper left or the upper right corner, then returning to start position. The order of targets was determined beforehand to be interleaved pseudo-randomly and was communicated

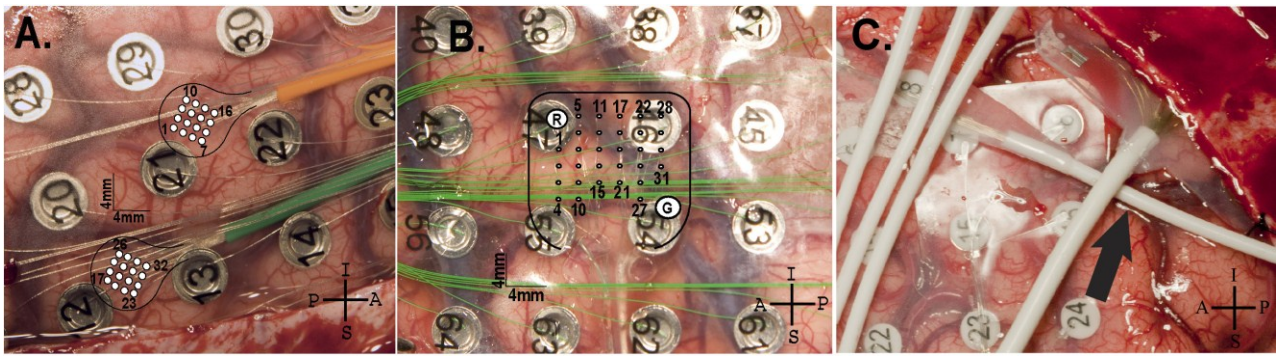

Figure 1. Implant pictures. (Left) Two 16-chan. µECoG arrays (1-mm spacing) were implanted over hand area (orange wire) and arm area (green wire) right primary motor cortex in P1. (Middle) A single 30-chan. array (2-mm spacing) was implanted over left primary motor cortex hand and arm area in P2. (Right) A 64-chan. array (3-mm spacing) was implanted over hand and arm sensory and motor cortex; only the base is visible.

through the verbal cue. Trials lasted 2–3 seconds with a 1-second separation.

Patient P3 was instructed with a visual cue to move the cursor to one of two targets on each side of the monitor using a computer mouse. The sequence of target presentation was determined online by a pseudo-random algorithm.

C. Data Analysis

For P1 and P2, the tablet and array outputs were recorded with a NeuroPort system (Blackrock Microsystems, Salt Lake City, UT) at 2,000 samples/sec, or at 30,000 samples/sec and downsampled to 2 kS/sec. The data were also highpass filtered at 1 Hz to attenuate motion artifact. A total of 14 sessions were used for P1, and nine sessions for P2. Sessions were 117 ± 74 sec (P1) and 120 ± 61 sec (P2) in length.

Multitapered spectrograms between 0 and 500 Hz were generated using the Chronux package. The spectral data were averaged into frequency bins covering 0-5 Hz, 5-13 Hz, 13-30 Hz, 30-80 Hz, 80-200 Hz, and 200-500 Hz. All frequencies within ±5 Hz of 60 Hz or its harmonics were removed due to line noise contamination. The movement data were downsampled to the same sampling rate as the spectrograms moving window rate (4 samples/sec). An offset of 150 msec was introduced between the movement data and the spectral data to model delay between neural activity and motor output. The final feature vector z_k consisted of 6 frequency bins per channel and the hand state x_k was represented by a six-dimensional vector comprising x and y position, velocity, and acceleration for k = 1, 2, … M, where M was the number of samples in the data set.

A standard Kalman filter was implemented to perform the trajectory decode [6]. The likelihood model was defined as

$$z_k = H_k x_k + q_k \quad (1)$$

where H_k linearly relates the hand kinematics x_k to the neural features z_k, and q_k represents noise in the observation, assumed to be zero-mean and normally distributed with covariance matrix Q_k. Next, the state transformation matrix, A_k, was defined to model how the system state, i.e., the hand kinematics, varied over time, with w_k, a noise term, also assumed to be zero-mean and normally distributed with covariance matrix W_k.

$$x_{k+1} = A_k x_k + w_k \quad (2)$$

Neural data recorded during two different task sessions were used for training and testing. The parameters A, H, W, and Q were directly calculated from the training data as described in [6] and were assumed to be constant, e.g., A_k = A. Additionally, the means of the movement and neural data features were calculated in order to center the data, and the data were orthogonalized using PCA, with tailing principal components contributing less than 1% of the variance discarded. The principal components and means found during training were applied to the testing data to mimic realtime constraints.

To determine the level of chance in the context of the continuous trajectory decode, the Kalman filter was trained and tested using zero-mean white noise in place of the neural data (but maintaining the kinematic data). The level of chance was estimated as the average correlation across all combinations of training and testing sessions using this white noise.

For P3, the Kalman filter was implemented in real-time. The decode was trained using one minute of data recorded during reaches to two horizontal targets randomly cued. During this training, 18 channels on the grid were used for the decode. These channels were chosen because the neural data from these channels demonstrated moderate correlations with arm movement. For the selected channels, spectral data was averaged between 20-30 Hz. 100 ms time bins were used, with an offset of 200 msec between neural data and kinematics. The position of the cursor during online decoding was restricted within the space of the tablet and monitor, but no algorithmic constraints were applied to trajectory.

III. Results

A. Decoding Arm Trajectories

As an initial step to verify that there was some basis to the Kalman filtering approach, each task session was used as both the training and the test set. The correlation between the Kalman filter's predicted hand position and the actual

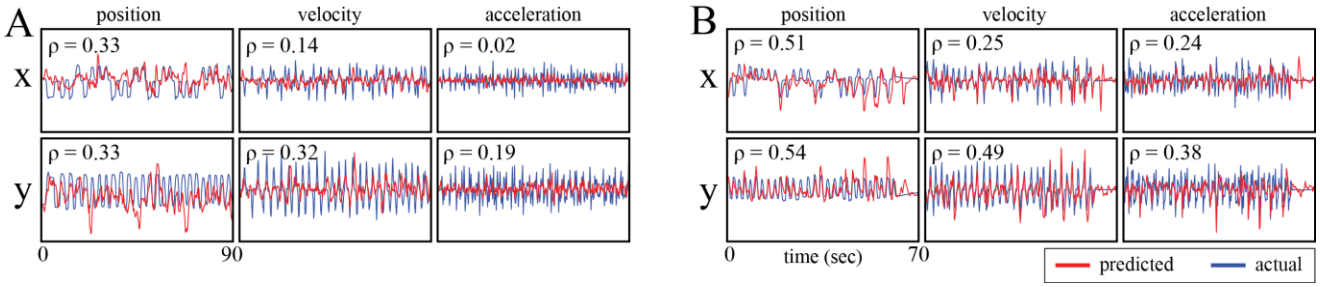

Figure 2. Sample output of the Kalman filter for patients P1 and P2. In Panel A, the Kalman filter was trained on 113 seconds of data recorded during an experimental session with P1, then tested on 90 seconds of data recorded during a subsequent experimental session which began 226 seconds after the first session ended. In Panel B, the Kalman filter was trained on 55 seconds of data recorded during an experimental session with P2, then tested on 70 seconds of data recorded during a subsequent session which began 15 seconds after the first session ended.

TABLE I. LEVEL OF CHANCE FOR ALL KINEMATIC VARIABLES, FOR EACH PATIENT.

	x-pos	*y-pos*	*x-vel*	*y-vel*	*x-acc*	*y-acc*
P1	0.08	0.08	0.06	0.06	0.04	0.04
P2	0.09	0.07	0.06	0.06	0.05	0.04

position were calculated to evaluate performance. With the same data used for both training and testing, the mean and standard deviation of the correlations for x- and y-position of P1 was 0.76 ± 0.18 and 0.78 ± 0.17 respectively; for P2 they were 0.76 ±0.16 and 0.73 ±0.14, respectively. That the parameters A, H, W, and Q could be learned and then statically reapplied to the data implies that linear relationships persisted, at least on this short time scale, between hand kinematics and the neural data.

Performance was lower (Fig. 2) when the Kalman filter was run on separate data for training and testing, although in most cases the performance was well above chance (Table 1). To evaluate the performance of the Kalman filter, all possible pairs of task sessions were used as training and testing sets for each patient, under the constraint that the test set occurred subsequent to the training set. With 14 task sessions for P1, there were 91 possible training and testing pairs; for P2, there were nine task sessions and 36 possible pairs. The mean and standard deviation of x-position correlation across these pairings was 0.13 ± 0.10 for P1 (48 of 91, or 52.7% above chance) and 0.19 ± 0.15 for P2 (27 of 36, or 75.0% above chance). For the y-position, correlations were 0.16 ± 0.12 for P1 (65 of 91, or 71.4% above chance) and 0.22 ± 0.19 for P2 (25 of 36, or 69.4% above chance). For P1, 11 of 91 combinations resulted in correlations above the level of chance for all six kinematic variables; 38 of 91 combinations resulted in correlations above the level of chance for just the position variables. For P2, 12 of 36 combinations were above chance for all six kinematic variables, and 20 of 36 combinations were above the level of chance in both dimensions of position (Fig. 3).

If the pairs were further constrained such that only consecutive task sessions were used for training and testing, the performance increased: x-position correlations were 0.17 ± 0.13 for P1 and 0.23 ± 0.18 for P2, and y-position correlations were 0.21 ±0.12 for P1 and 0.25 ± 0.20 for P2. Some pairs demonstrated much higher correlations. The maximums for P1 were 0.39 and 0.49 for x- and y-position, respectively. The maximums for P2 were 0.59 and 0.59, respectively.

P3 controlled the movement of a cursor on the screen using the real-time Kalman filter, moving the cursor between targets based on visual cues for 21 minutes (Figure 4). On average, P3 required 2.15 seconds to start moving in the direction of the target, and (in total) 6.24 seconds to acquire each target. All presented targets were acquired.

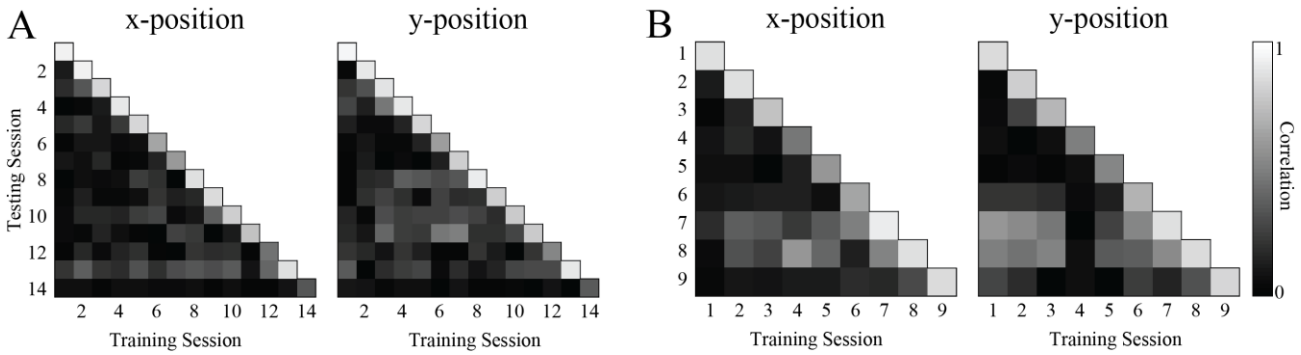

Figure 3. Summary of performance of the Kalman filter for P1 and P2. Panel A shows results for P1; Panel B shows results for P2. Only combinations of experimental sessions in which testing sessions occurred after training sessions were used as training and testing pairs (thus the blank upper triangles), with the correlation between actual and predicted x and y positions shown in these images. The color scale indicates the magnitude of the correlation between 0 and 1. The diagonal indicates the performance when training and testing on the same data.

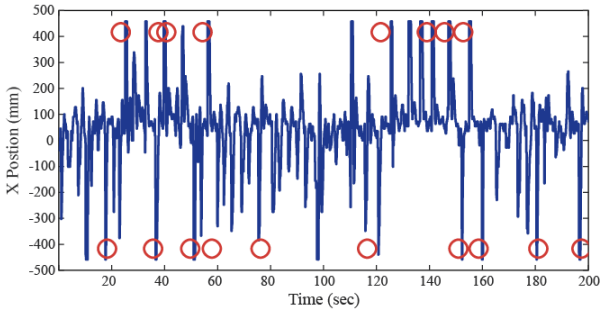

Figure 4. X position of cursor on a computer monitor controlled by P3 with the real-time Kalman filter. The blue line represents the x position in millimeters of the cursor as P3 was randomly cued to move to two targets (red circles) horizontally separated on the monitor. A single feature was used from 18 channels, consisting of the average power between 20 and 30 Hz. The real-time Kalman filter was trained for 1 minute and was implemented with 100 ms time bins and a -200ms time lag.

IV. Discussion

This study was designed to investigate whether a µECoG grid could serve as brain-computer interface (BCI) for a motor neural prosthesis. The results described here demonstrate above-chance performance in an offline environment when decoding arm trajectories from microelectrodes resting over primary motor cortex. Furthermore, these results demonstrate that real-time control of a cursor on a computer screen is possible using surface local field potentials.

It is likely that there is significant motor information represented at the scale of single cortical columns. It is possible that a µECoG grid may be capable of acquiring local field potential signals at this scale from the surface of the cortex. Extracting neural information at this spatial scale may be necessary to provide dexterous intuitive control of a prosthesis. At one extreme, accurate control for fine movements of an external device might require wires with subcolumnar (less than 1000 micron) spacing. Such a system could approach the scale and quality of local field potentials recorded with penetrating microelectrodes. At another extreme, it is possible that nonpenetrating wires could only accurately measure an "ECoG-like" integrated signal from a broad region of cortex. If the information content available at the pial surface is substantially spatially limited, perhaps to a range of several millimeters, then the best motor decode possible using a µECoG grid may not substantially differ from what is possible through a conventional ECoG grid or possibly epidural electrodes.

This study demonstrated that continuous trajectory decodes are possible using cortical surface potentials recorded over motor cortex with dense grids of microelectrodes. While continuous trajectories have been decoded previously using intracortical field potentials [7, 8], and macroscale surface potentials [8, 9], this is the first work to demonstrate the concept using surface local field potentials. Significant work remains to improve the accuracy and performance of the trajectory decode. Specifically, adaptive methods could be applied to a number of aspects of the decode process, for example, to update the means and principal components online, and to update the parameters A, H, W, and Q to reflect changing relationships in the neural data over time. Furthermore, although the linear models used for this work were sufficient for demonstration, the true nature of the relationship between motor output and neural activity is likely to be nonlinear. As these issues continue to be explored, the extended Kalman filter, which allows for nonlinear models, may become more appropriate.

V. Conclusion

The primary finding of this study is that brain activity recorded at a millimeter scale from the cortical surface supports motor-BCI applications. By providing high spatial resolution electrophysiological recordings of human neocortical activity, µECoG arrays may be able to serve as an interface that provides dexterous intuitive control of a limb prosthesis. Additionally, this technology may serve as a novel research tool for studying spatially local neocortical phenomena in health and disease.

References

[1] J. J. Van Gompel, S. M. Stead, C. Giannini, F. B. Meyer, W. R. Marsh, T. Fountain, E. So, A. Cohen-Gadol, K. H. Lee, and G. A. Worrell, "Phase I trial: safety and feasibility of intracranial electroencephalography using hybrid subdural electrodes containing macro- and microelectrode arrays," *Neurosurg Focus,* vol. 25, p. E23, Sep 2008.

[2] G. A. Worrell, A. B. Gardner, S. M. Stead, S. Hu, S. Goerss, G. J. Cascino, F. B. Meyer, R. Marsh, and B. Litt, "High-frequency oscillations in human temporal lobe: simultaneous microwire and clinical macroelectrode recordings," *Brain,* vol. 131, pp. 928-37, Apr 2008.

[3] S. S. Kellis, P. A. House, K. E. Thomson, R. Brown, and B. Greger, "Human neocortical electrical activity recorded on nonpenetrating microwire arrays: applicability for neuroprostheses," *Neurosurg Focus,* vol. 27, p. E9, Jul 2009.

[4] S. Kellis, K. Miller, K. Thomson, R. Brown, P. House, and B. Greger, "Decoding spoken words using local field potentials recorded from the cortical surface," *J Neural Eng,* vol. 7, p. 056007, Oct 2010.

[5] J. P. Cunningham, P. Nuyujukian, V. Gilja, C. A. Chestek, S. I. Ryu, and K. V. Shenoy, "A closed-loop human simulator for investigating the role of feedback control in brain-machine interfaces," *J Neurophysiol,* vol. 105, pp. 1932-49, Apr 2011.

[6] W. Wu, Y. Gao, E. Bienenstock, J. P. Donoghue, and M. J. Black, "Bayesian Population Decoding of Motor Cortical Activity Using a Kalman Filter," *Neural Computation,* vol. 18, pp. 80-118, 2006/01/01 2006.

[7] Z. Jun, W. Truccolo, C. Vargas-Irwin, and J. P. Donoghue, "Decoding 3-D Reach and Grasp Kinematics From High-Frequency Local Field Potentials in Primate Primary Motor Cortex," *Biomedical Engineering, IEEE Transactions on,* vol. 57, pp. 1774-1784, 2010.

[8] L. Srinivasan, U. T. Eden, S. K. Mitter, and E. N. Brown, "General-Purpose Filter Design for Neural Prosthetic Devices," *Journal of Neurophysiology,* vol. 98, pp. 2456-2475, October 1, 2007 2007.

[9] T. Pistohl, T. Ball, A. Schulze-Bonhage, A. Aertsen, and C. Mehring, "Prediction of arm movement trajectories from ECoG-recordings in humans," *Journal of Neuroscience Methods,* vol. 167, pp. 105-114, 2008.